EUROPEAN ORGANIZATION FOR NUCLEAR RESEARCH

CERN-EP/2003-039
11 July 2003

Measurement of Heavy Quark Forward-Backward Asymmetries and Average B Mixing Using Leptons in Hadronic Z Decays

The OPAL Collaboration

Abstract

A measurement of the forward-backward asymmetries of $e^+e^- \to b\overline{b}$ and $e^+e^- \to c\overline{c}$ events using electrons and muons produced in semileptonic decays of bottom and charm hadrons is presented. The outputs of two neural networks designed to identify $b \to \ell^-$ and $c \to \ell^+$ decays are used in a maximum likelihood fit to a sample of events containing one or two identified leptons. The b and c quark forward-backward asymmetries at three centre-of-mass energies $\sqrt{s}$ and the average B mixing parameter $\overline{\chi}$ are determined simultaneously in the fit. Using all data collected by OPAL near the Z resonance, the asymmetries are measured to be:

$$\begin{array}{llll} A_{\rm FB}^{b\overline{b}} = (\ 4.7\ \pm 1.8\ \pm 0.1\ )\,\% & A_{\rm FB}^{c\overline{c}} = (-6.8\ \pm 2.5\ \pm 0.9\ )\,\% & \text{at } \langle\sqrt{s}\rangle = 89.51 \text{ GeV}, \\ A_{\rm FB}^{b\overline{b}} = (\ 9.72 \pm 0.42 \pm 0.15)\,\% & A_{\rm FB}^{c\overline{c}} = (\ 5.68 \pm 0.54 \pm 0.39)\,\% & \text{at } \langle\sqrt{s}\rangle = 91.25 \text{ GeV}, \\ A_{\rm FB}^{b\overline{b}} = (10.3\ \pm 1.5\ \pm 0.2\ )\,\% & A_{\rm FB}^{c\overline{c}} = (\ 14.6\ \pm 2.0\ \pm 0.8\ )\,\% & \text{at } \langle\sqrt{s}\rangle = 92.95 \text{ GeV}. \end{array}$$

For the average B mixing parameter, a value of:

$$\overline{\chi} = (13.12 \pm 0.49 \pm 0.42)\,\%$$

is obtained. In each case the first uncertainty is statistical and the second systematic. These results are combined with other OPAL measurements of the b and c forward-backward asymmetries, and used to derive a value for the effective electroweak mixing angle for leptons $\sin^2\theta^\ell_{\rm eff}$ of 0.23238 ± 0.00052.

Submitted to Phys. Lett. B

The OPAL Collaboration

G. Abbiendi[2], C. Ainsley[5], P.F. Åkesson[3], G. Alexander[22], J. Allison[16], P. Amaral[9], G. Anagnostou[1], K.J. Anderson[9], S. Arcelli[2], S. Asai[23], D. Axen[27], G. Azuelos[18,a], I. Bailey[26], E. Barberio[8,p], R.J. Barlow[16], R.J. Batley[5], P. Bechtle[25], T. Behnke[25], K.W. Bell[20], P.J. Bell[1], G. Bella[22], A. Bellerive[6], G. Benelli[4], S. Bethke[32], O. Biebel[31], O. Boeriu[10], P. Bock[11], M. Boutemeur[31], S. Braibant[8], L. Brigliadori[2], R.M. Brown[20], K. Buesser[25], H.J. Burckhart[8], S. Campana[4], R.K. Carnegie[6], B. Caron[28], A.A. Carter[13], J.R. Carter[5], C.Y. Chang[17], D.G. Charlton[1], A. Csilling[29], M. Cuffiani[2], S. Dado[21], A. De Roeck[8], E.A. De Wolf[8,s], K. Desch[25], B. Dienes[30], M. Donkers[6], J. Dubbert[31], E. Duchovni[24], G. Duckeck[31], I.P. Duerdoth[16], E. Etzion[22], F. Fabbri[2], L. Feld[10], P. Ferrari[8], F. Fiedler[31], I. Fleck[10], M. Ford[5], A. Frey[8], A. Fürtjes[8], P. Gagnon[12], J.W. Gary[4], G. Gaycken[25], C. Geich-Gimbel[3], G. Giacomelli[2], P. Giacomelli[2], M. Giunta[4], J. Goldberg[21], E. Gross[24], J. Grunhaus[22], M. Gruwé[8], P.O. Günther[3], A. Gupta[9], C. Hajdu[29], M. Hamann[25], G.G. Hanson[4], K. Harder[25], A. Harel[21], M. Harin-Dirac[4], M. Hauschild[8], C.M. Hawkes[1], R. Hawkings[8], R.J. Hemingway[6], C. Hensel[25], G. Herten[10], R.D. Heuer[25], J.C. Hill[5], K. Hoffman[9], D. Horváth[29,c], P. Igo-Kemenes[11], K. Ishii[23], H. Jeremie[18], P. Jovanovic[1], T.R. Junk[6], N. Kanaya[26], J. Kanzaki[23,u], G. Karapetian[18], D. Karlen[26], K. Kawagoe[23], T. Kawamoto[23], R.K. Keeler[26], R.G. Kellogg[17], B.W. Kennedy[20], D.H. Kim[19], K. Klein[11,t], A. Klier[24], S. Kluth[32], T. Kobayashi[23], M. Kobel[3], S. Komamiya[23], L. Kormos[26], T. Krämer[25], P. Krieger[6,l], J. von Krogh[11], K. Kruger[8], T. Kuhl[25], M. Kupper[24], G.D. Lafferty[16], H. Landsman[21], D. Lanske[14], J.G. Layter[4], A. Leins[31], D. Lellouch[24], J. Letts[o], L. Levinson[24], J. Lillich[10], S.L. Lloyd[13], F.K. Loebinger[16], J. Lu[27,w], J. Ludwig[10], A. Macpherson[28,i], W. Mader[3], S. Marcellini[2], A.J. Martin[13], G. Masetti[2], T. Mashimo[23], P. Mättig[m], W.J. McDonald[28], J. McKenna[27], T.J. McMahon[1], R.A. McPherson[26], F. Meijers[8], W. Menges[25], F.S. Merritt[9], H. Mes[6,a], A. Michelini[2], S. Mihara[23], G. Mikenberg[24], D.J. Miller[15], S. Moed[21], W. Mohr[10], T. Mori[23], A. Mutter[10], K. Nagai[13], I. Nakamura[23,V], H. Nanjo[23], H.A. Neal[33], R. Nisius[32], S.W. O'Neale[1], A. Oh[8], A. Okpara[11], M.J. Oreglia[9], S. Orito[23,*], C. Pahl[32], G. Pásztor[4,g], J.R. Pater[16], G.N. Patrick[20], J.E. Pilcher[9], J. Pinfold[28], D.E. Plane[8], B. Poli[2], J. Polok[8], O. Pooth[14], M. Przybycień[8,n], A. Quadt[3], K. Rabbertz[8,r], C. Rembser[8], P. Renkel[24], J.M. Roney[26], S. Rosati[3], Y. Rozen[21], K. Runge[10], K. Sachs[6], T. Saeki[23], E.K.G. Sarkisyan[8,j], A.D. Schaile[31], O. Schaile[31], P. Scharff-Hansen[8], J. Schieck[32], T. Schörner-Sadenius[8], M. Schröder[8], M. Schumacher[3], C. Schwick[8], W.G. Scott[20], R. Seuster[14,f], T.G. Shears[8,h], B.C. Shen[4], P. Sherwood[15], G. Siroli[2], A. Skuja[17], A.M. Smith[8], R. Sobie[26], S. Söldner-Rembold[16,d], F. Spano[9], A. Stahl[3], K. Stephens[16], D. Strom[19], R. Ströhmer[31], S. Tarem[21], M. Tasevsky[8], R.J. Taylor[15], R. Teuscher[9], M.A. Thomson[5], E. Torrence[19], D. Toya[23], P. Tran[4], I. Trigger[8], Z. Trócsányi[30,e], E. Tsur[22], M.F. Turner-Watson[1], I. Ueda[23], B. Ujvári[30,e], C.F. Vollmer[31], P. Vannerem[10], R. Vértesi[30], M. Verzocchi[17], H. Voss[8,q], J. Vossebeld[8,h], D. Waller[6], C.P. Ward[5], D.R. Ward[5], P.M. Watkins[1], A.T. Watson[1], N.K. Watson[1], P.S. Wells[8], T. Wengler[8], N. Wermes[3], D. Wetterling[11] G.W. Wilson[16,k], J.A. Wilson[1], G. Wolf[24], T.R. Wyatt[16], S. Yamashita[23], D. Zer-Zion[4], L. Zivkovic[24]

[1]School of Physics and Astronomy, University of Birmingham, Birmingham B15 2TT, UK
[2]Dipartimento di Fisica dell' Università di Bologna and INFN, I-40126 Bologna, Italy
[3]Physikalisches Institut, Universität Bonn, D-53115 Bonn, Germany
[4]Department of Physics, University of California, Riverside CA 92521, USA
[5]Cavendish Laboratory, Cambridge CB3 0HE, UK
[6]Ottawa-Carleton Institute for Physics, Department of Physics, Carleton University, Ottawa, Ontario K1S 5B6, Canada
[8]CERN, European Organisation for Nuclear Research, CH-1211 Geneva 23, Switzerland
[9]Enrico Fermi Institute and Department of Physics, University of Chicago, Chicago IL 60637, USA
[10]Fakultät für Physik, Albert-Ludwigs-Universität Freiburg, D-79104 Freiburg, Germany
[11]Physikalisches Institut, Universität Heidelberg, D-69120 Heidelberg, Germany

[12]Indiana University, Department of Physics, Bloomington IN 47405, USA
[13]Queen Mary and Westfield College, University of London, London E1 4NS, UK
[14]Technische Hochschule Aachen, III Physikalisches Institut, Sommerfeldstrasse 26-28, D-52056 Aachen, Germany
[15]University College London, London WC1E 6BT, UK
[16]Department of Physics, Schuster Laboratory, The University, Manchester M13 9PL, UK
[17]Department of Physics, University of Maryland, College Park, MD 20742, USA
[18]Laboratoire de Physique Nucléaire, Université de Montréal, Montréal, Québec H3C 3J7, Canada
[19]University of Oregon, Department of Physics, Eugene OR 97403, USA
[20]CLRC Rutherford Appleton Laboratory, Chilton, Didcot, Oxfordshire OX11 0QX, UK
[21]Department of Physics, Technion-Israel Institute of Technology, Haifa 32000, Israel
[22]Department of Physics and Astronomy, Tel Aviv University, Tel Aviv 69978, Israel
[23]International Centre for Elementary Particle Physics and Department of Physics, University of Tokyo, Tokyo 113-0033, and Kobe University, Kobe 657-8501, Japan
[24]Particle Physics Department, Weizmann Institute of Science, Rehovot 76100, Israel
[25]Universität Hamburg/DESY, Institut für Experimentalphysik, Notkestrasse 85, D-22607 Hamburg, Germany
[26]University of Victoria, Department of Physics, P O Box 3055, Victoria BC V8W 3P6, Canada
[27]University of British Columbia, Department of Physics, Vancouver BC V6T 1Z1, Canada
[28]University of Alberta, Department of Physics, Edmonton AB T6G 2J1, Canada
[29]Research Institute for Particle and Nuclear Physics, H-1525 Budapest, P O Box 49, Hungary
[30]Institute of Nuclear Research, H-4001 Debrecen, P O Box 51, Hungary
[31]Ludwig-Maximilians-Universität München, Sektion Physik, Am Coulombwall 1, D-85748 Garching, Germany
[32]Max-Planck-Institute für Physik, Föhringer Ring 6, D-80805 München, Germany
[33]Yale University, Department of Physics, New Haven, CT 06520, USA

[a] and at TRIUMF, Vancouver, Canada V6T 2A3
[c] and Institute of Nuclear Research, Debrecen, Hungary
[d] and Heisenberg Fellow
[e] and Department of Experimental Physics, Lajos Kossuth University, Debrecen, Hungary
[f] and MPI München
[g] and Research Institute for Particle and Nuclear Physics, Budapest, Hungary
[h] now at University of Liverpool, Dept of Physics, Liverpool L69 3BX, U.K.
[i] and CERN, EP Div, 1211 Geneva 23
[j] and Manchester University
[k] now at University of Kansas, Dept of Physics and Astronomy, Lawrence, KS 66045, U.S.A.
[l] now at University of Toronto, Dept of Physics, Toronto, Canada
[m] current address Bergische Universität, Wuppertal, Germany
[n] now at University of Mining and Metallurgy, Cracow, Poland
[o] now at University of California, San Diego, U.S.A.
[p] now at Physics Dept Southern Methodist University, Dallas, TX 75275, U.S.A.
[q] now at IPHE Université de Lausanne, CH-1015 Lausanne, Switzerland
[r] now at IEKP Universität Karlsruhe, Germany
[s] now at Universitaire Instelling Antwerpen, Physics Department, B-2610 Antwerpen, Belgium
[t] now at RWTH Aachen, Germany
[u] and High Energy Accelerator Research Organisation (KEK), Tsukuba, Ibaraki, Japan
[v] now at University of Pennsylvania, Philadelphia, Pennsylvania, USA
[w] now at TRIUMF, Vancouver, Canada
[*] Deceased

1 Introduction

The measurement of the forward-backward asymmetries of heavy quarks, $A_{\rm FB}^{\rm q\overline{q}}$ (q=b,c), in $\rm e^+e^- \to q\overline{q}$ events provides an important test of the Standard Model. The $\rm b\overline{b}$ forward-backward asymmetry provides one of the most precise determinations of the effective electroweak mixing angle for leptons $\sin^2\theta^\ell_{\rm eff}$ (assuming lepton universality). This is of particular interest at the present time in view of the nearly three standard deviation difference between the average values of $\sin^2\theta^\ell_{\rm eff}$ derived from quark forward-backward asymmetries at LEP on the one hand and from lepton forward-backward asymmetries at LEP and the left-right asymmetry at SLD on the other [1].

The forward-backward asymmetry arises from the $\cos\theta$ term in the differential cross-section for $\rm e^+e^- \to q\overline{q}$,

$$\frac{\mathrm{d}\sigma}{\mathrm{d}\cos\theta} \propto 1 + \cos^2\theta + \frac{8}{3} A_{\rm FB}^{\rm q\overline{q}} \ \cos\theta \,, \tag{1}$$

where θ denotes the angle between the outgoing quark and the incoming electron flight directions, and where initial and final state radiation, quark mass effects and higher order terms have been neglected. The asymmetry $A_{\rm FB}^{\rm q\overline{q}}$ is related to the vector, $g_{\rm V}$, and axial-vector, $g_{\rm A}$, couplings of the Z to the electron e and quark q. At the peak of the Z resonance and for the s-channel Z exchange process only, the pole asymmetry is given by

$$A_{\rm FB}^{0,\rm q} \equiv \frac{3}{4}\mathcal{A}_{\rm e}\mathcal{A}_{\rm q} = \frac{3}{4} \ \frac{2g_{\rm Ve}/g_{\rm Ae}}{1+(g_{\rm Ve}/g_{\rm Ae})^2} \ \frac{2g_{\rm Vq}/g_{\rm Aq}}{1+(g_{\rm Vq}/g_{\rm Aq})^2} \,. \tag{2}$$

In the Standard Model the couplings for any fermion f are related to the fermion charge $Q_{\rm f}$ and its effective electroweak mixing angle $\sin^2\theta^{\rm f}_{\rm eff}$ as follows:

$$\frac{g_{\rm Vf}}{g_{\rm Af}} = (1 - 4|Q_{\rm f}|\sin^2\theta^{\rm f}_{\rm eff}) \,. \tag{3}$$

The values of $\sin^2\theta^{\rm f}_{\rm eff}$ are all close to 0.25, so the value of the asymmetry parameter for electrons, $\mathcal{A}_{\rm e}$, is small, and varies rapidly with $\sin^2\theta^\ell_{\rm eff}$, but the value of $\mathcal{A}_{\rm b}$ is large, approximately 0.94, and varies only slowly with $\sin^2\theta^{\rm b}_{\rm eff}$. This results in a relatively large forward-backward asymmetry for $\rm b\overline{b}$ events, which is then very sensitive to $\sin^2\theta^\ell_{\rm eff}$ via $\mathcal{A}_{\rm e}$.

This analysis uses hadronic Z decays observed by the OPAL detector at LEP to measure $A_{\rm FB}^{\rm b\overline{b}}$ and $A_{\rm FB}^{\rm c\overline{c}}$. The event thrust axis is used to estimate the primary quark direction. Leptons produced in semileptonic decays of b and c hadrons, usually referred to as prompt leptons, are used to identify heavy flavour events, and their charge is used to distinguish between decaying quarks and antiquarks. The asymmetry for $\rm b\overline{b}$ events is diluted by the effect of neutral B meson mixing [2]. This is quantified by the average mixing parameter, $\overline{\chi}$, which is the probability that a produced b hadron decays as its antiparticle. The effect of B mixing is to reduce the observed asymmetry of $\rm b\overline{b}$ events by a factor $(1-2\overline{\chi})$ with respect to the asymmetry without mixing. The parameter $\overline{\chi}$ can be measured from the fraction of like-sign lepton pairs in events with an identified lepton in each hemisphere of the event. The b and c asymmetries, and the mixing parameter $\overline{\chi}$, are therefore measured in a simultaneous fit to events with one or two identified leptons. The contributions of $\rm b\overline{b}$ and $\rm c\overline{c}$ events to the lepton samples are separated from each other and from background by using several kinematic variables describing the lepton and its associated jet, combined using neural network flavour separation algorithms.

This paper supersedes our previous publication [3]. Compared to the previous paper, this analysis benefits from the inclusion of data recorded after 1994, and from a reprocessing of the full OPAL data set with final tracking algorithms and detector calibrations, which have improved in particular the performance of the electron identification and flavour separation algorithms. The systematic uncertainties have been reduced due to better knowledge of heavy flavour production and decay, and several details of the fit have also been improved. Similar analyses have been published by the other LEP experiments [4, 5, 6]. Analyses identifying b quark events via the resolvable decay length of b hadrons [7, 8, 9, 10] also give precise measurements of the b quark forward-backward asymmetry. In addition, the charm asymmetry has been measured using reconstructed charm hadrons [11, 12, 13].

2 Data sample and event simulation

The OPAL detector is described in detail elsewhere [14,15,16]. The central tracking system is located inside a solenoid which provides a uniform axial magnetic field of 0.435 T along the beam axis. The beam axis coincides with the z-axis of the detector, with the polar angle θ measured with respect to the direction of the electron beam. The azimuthal angle ϕ is measured around the z-axis, and the radius r is the distance from the z-axis. The innermost part of the tracking system is a two-layer silicon micro-vertex detector. The silicon detector is surrounded by a vertex drift chamber, a large volume jet chamber with 159 layers of axial anode wires and a set of z chambers measuring the track coordinates along the beam direction. The jet chamber also provides a measurement of the rate of energy deposition along the track, $\mathrm{d}E/\mathrm{d}x$.

Outside the magnet coil, the tracking system is surrounded by a lead-glass electromagnetic calorimeter. The barrel region covers the polar angle range $|\cos\theta| < 0.82$, and full acceptance to $|\cos\theta| < 0.98$ is provided by the endcaps. The iron return yoke and pole pieces of the magnet are instrumented with streamer tubes and thin multiwire chambers to act as a hadronic calorimeter. The calorimeters are surrounded by muon chambers.

Some flavour separation aspects of this analysis exploit the long lifetimes of b and c hadrons, and therefore rely in particular on the silicon microvertex detector. This detector was first operational in 1991, providing measurements in the r-ϕ plane only. In 1993 it was upgraded to measure tracks in both r-ϕ and r-z planes [15], and in 1996 the $\cos\theta$ coverage for at least one silicon measurement was extended from $|\cos\theta| < 0.83$ to $|\cos\theta| < 0.93$ [16]. The changing detector performance with time was taken into account in the analysis. The resolution of the vertex drift chamber is sufficient to ensure some flavour separation even in data taken without silicon microvertex detector information.

Hadronic Z decays were selected using standard criteria, as in [17]. All the LEP1 data collected at centre-of-mass energies close to the peak of the Z resonance between 1990 and 1995 were included, together with Z–peak data recorded for detector calibration purposes during the higher energy LEP2 running between 1996 and 2000. The thrust axis direction was calculated using charged particle tracks and electromagnetic calorimeter clusters not associated to any track. The polar angle of the thrust axis θ_{T} was required to satisfy $|\cos\theta_{\mathrm{T}}| < 0.95$. Over four million hadronic events were selected. The exact numbers are listed in Table 1. As indicated in the table, some events were recorded at centre-of-mass energies above and below the Z peak. The bulk of these off-peak data were recorded in 1993 and 1995 at centre-of-mass energies approximately 1.8 GeV away from the peak. The other off-peak centre-of-mass energy samples from 1990 and 1991 are combined with these main samples, yielding measurements of the forward-backward asymmetries at three separate energy points.

Mean Energy of Z events	Selected Z decays	Single lepton events		Dilepton events
		Electrons	Muons	
peak–2 $\langle\sqrt{s}\rangle = 89.51$ GeV	194 211	11 567	19 809	321
peak $\langle\sqrt{s}\rangle = 91.25$ GeV	4 079 047	239 505	410 877	6 014
peak+2 $\langle\sqrt{s}\rangle = 92.95$ GeV	278 257	16 977	30 066	394

Table 1: The number of events selected below, on and above the Z peak. The average centre-of-mass energies of the selected Z events, the numbers of Z events, and the numbers of events with identified leptons are shown. Note that dilepton events are only selected in a region of high b-purity.

Monte Carlo simulated events were generated using JETSET 7.4 [18] with parameters tuned by OPAL [19]. The fragmentation function of Peterson *et al.* [20] was used to describe the fragmentation of b and c quarks. The semileptonic decay model of Altarelli *et al.* [21] with parameters fixed by CLEO, DELCO and MARKIII data [22,23,24] was used to predict the lepton momentum in the rest frame of b and c hadrons. The generated events were passed through a program that simulated the response of the OPAL detector [25] and through the same reconstruction algorithms as the data.

3 Lepton identification and flavour separation

Leptons were identified in hadronic events using well established algorithms [17]. All tracks with momentum greater than 2 GeV and $|\cos\theta| < 0.96$ were considered as lepton candidates.

Electron candidate tracks were required to have at least 20 measurements of $\mathrm{d}E/\mathrm{d}x$ from jet chamber hits. Electrons were then identified using a neural network algorithm. The identification relies on ionisation energy loss ($\mathrm{d}E/\mathrm{d}x$) measured in the tracking chamber, together with spatial and energy-momentum (E/p) matching between tracking and calorimetry. The neural network output was in the range 0 to 1, and was required to be greater than 0.9 for electron candidates. Photon conversions were rejected using another neural network algorithm [17]. The efficiency of this selection for genuine electrons, not considering electrons from photon conversions, is 66 %. The purity is 73 %, where photon conversions are included in the background.

Muons were identified by requiring a spatial match between a track reconstructed in the tracking detectors and a track segment reconstructed in the external muon chambers. Further rejection of kaons was achieved with loose $\mathrm{d}E/\mathrm{d}x$ cuts [17]. These requirements selected muons with an efficiency of 74 % and a purity of 53 %.

In this analysis, only leptons from the decay of a b or c hadron in a primary $\mathrm{b\overline{b}}$ or $\mathrm{c\overline{c}}$ event are considered as signal. Any other genuine electron or muon, and any hadron misidentified as a lepton, is considered as background. With this definition, about 11 % of the electron background is from genuine electrons in light quark events, 49 % from misidentified hadrons in any primary quark flavour event, and 40 % from photon conversions. About 68 % of the muon background originates from pions, and 28 % from kaons.

The relationship between the lepton charge and the primary quark or antiquark from whose decay it originated is vital for the asymmetry measurement. Leptons coming directly from the weak decay of b hadrons are denoted $\mathrm{b} \to \ell^-$. A negatively-charged lepton comes from the decay of a hadron containing a b quark, and a positive lepton from a b antiquark[1]. Electrons and muons from leptonic τ decays where the τ lepton comes from a direct b decay, $\mathrm{b} \to \tau^- \to \ell^-$, have the same sign correlation as the $\mathrm{b} \to \ell^-$ events. Both lepton charges are possible if a b hadron decays to a c hadron, which then decays semileptonically. These decays are written as $\mathrm{b} \to \mathrm{c} \to \ell^+$ and $\mathrm{b} \to \overline{\mathrm{c}} \to \ell^-$, according to the charm content of the intermediate meson, and are both called cascade decays. In this analysis, any identified leptons from $\mathrm{c\overline{c}}$ mesons, e.g. $\mathrm{J}/\psi \to \ell^+\ell^-$ decays, are included with the cascades of the appropriate sign. A neutral B meson may have mixed before decay, so that a primary b quark decays as a b antiquark, or vice versa. Leptons from these mixed mesons are classified according to the decaying b quark, and contribute to the asymmetry with the wrong sign for their category, causing a reduction in the observed $\mathrm{b\overline{b}}$ asymmetry by a factor of $(1 - 2\overline{\chi})$. Leptons from the decay of c hadrons produced in $\mathrm{c\overline{c}}$ events, $\mathrm{c} \to \ell^+$, have the opposite sign correlation to direct $\mathrm{b} \to \ell^-$ decays; a primary c quark gives a positive lepton.

As in the previous analysis [3], two neural networks [26] denoted NETb and NETc were used to separate $\mathrm{b} \to \ell^-$ and $\mathrm{c} \to \ell^+$ decays from each other, from the cascade decays, $\mathrm{b} \to \mathrm{c} \to \ell^+$ and $\mathrm{b} \to \overline{\mathrm{c}} \to \ell^-$ which dilute the observed forward-backward asymmetries, and from backgrounds. The networks were retrained to take full advantage of the improved detector calibrations. Several of the network input variables refer to the jet containing the lepton track. The same tracks and clusters used to define the event thrust axis were combined into jets using a cone algorithm [27] with a cone half-angle of 0.55 rad and a minimum jet energy of 5.0 GeV. The transverse momentum, p_t, of each track was defined relative to the axis of the jet containing it, where the jet axis was calculated excluding the momentum of the track. A lepton sub-jet was defined as in [3]. The sub-jet includes particles that are nearer to the lepton than to the jet axis, and is a measure of the lepton isolation.

The first network, NETb, was trained to distinguish between $\mathrm{b} \to \ell^-$ events and all other categories. The input variables were the momentum p and transverse momentum p_t of the lepton candidate, the

[1] Charge conjugate decays are implied throughout this paper.

energy of the lepton sub-jet, $E_{\mathrm{sub-jet}}$, the total visible energy of the jet (calculated using all tracks and unassociated calorimeter clusters comprising the jet), $E^{\mathrm{vis}}_{\mathrm{jet}}$, and the scalar sum of the transverse momentum of all tracks within the jet, $(\sum p_t)_{\mathrm{jet}}$. Separate networks were trained for electrons and for muons. For the electron nets, two extra variables were included, namely the outputs of the electron and conversion neural networks. The distributions of the NETb output in the OPAL data are shown in Figure 1(a) and (b), together with the predictions from Monte Carlo; at high NETb values, the separation of $\mathrm{b} \to \ell^-$ events from all other lepton sources is clearly visible. For example, requiring NETb > 0.7 gives a sample 89 % pure in $\mathrm{b} \to \ell^-$ decays, with 3 % $\mathrm{b} \to \mathrm{c} \to \ell^+$ and 4 % $\mathrm{c} \to \ell^+$, whilst retaining 45 % of all $\mathrm{b} \to \ell^-$ decays with an identified lepton (averaged over electrons and muons). The Monte Carlo gives a reasonable description of the data, and the effect of the small discrepancies visible is discussed in Section 5.4.

The second network, NETc, was trained to distinguish $\mathrm{c} \to \ell^+$ events from all other categories, including $\mathrm{b} \to \ell^-$. The network used all the NETb variables, including the electron and conversion neutral network outputs for electron candidates, together with the following three quantities: the decay length significances, $(L/\sigma_L)_{1,2}$, of the jet containing the lepton (jet 1) and of the most energetic of the other jets in the event (jet 2), and the impact parameter significance of the lepton with respect to the primary vertex, d/σ_d. The decay length significance is the distance between the primary vertex and a secondary vertex, reconstructed from a subset of the tracks in the jet using the algorithms described in [17], divided by the error on the decay length. The impact parameter significance is the distance of closest approach of a track to the primary vertex, divided by its error. The distributions of the NETc output in the OPAL data are shown in Figure 1(c) and (d), together with the predictions from Monte Carlo; again the separation of $\mathrm{c} \to \ell^+$ events from other leptons is clearly visible. Requiring NETc > 0.7 gives a sample 59 % pure in $\mathrm{c} \to \ell^+$ decays, with 12 % $\mathrm{b} \to \ell^-$and 6 % $\mathrm{b} \to \mathrm{c} \to \ell^+$, whilst retaining 19 % of all $\mathrm{c} \to \ell^+$ decays with an identified lepton.

The values of NETb and NETc were evaluated for all lepton candidates. When more than one lepton was identified in an event, the candidates were ranked according to the value of NETb. If the best two lepton candidates in an event satisfied NETb > 0.6, and were in opposite thrust hemispheres, then both candidates were retained, and this was classified as a dilepton event. Otherwise only the best lepton candidate was considered, and the event was classified as a single lepton event. The numbers of single and dilepton events selected are given in Table 1.

4 Fit method and results

The values of the asymmetries and $\overline{\chi}$ were determined using a simultaneous fit to the observed numbers of single lepton events as a function of $\cos\theta_{\mathrm{T}}$, NETb and NETc, and the numbers of dilepton events as a function of $\cos\theta_{\mathrm{T}}$. The thrust axis of each event was used to estimate the direction of the primary quark, and the charge Q_ℓ of the identified leptons was used to distinguish between the quark and antiquark direction.

The total likelihood to be maximized is the product:

$$\mathcal{L} = \mathcal{L}_{\mathrm{single\ e}} \times \mathcal{L}_{\mathrm{single}\ \mu} \times \mathcal{L}_{\mathrm{double}} \ . \tag{4}$$

The single and double lepton likelihood terms are discussed in more detail below.

4.1 Single lepton likelihood

For single lepton events, the observable $y = -Q_\ell \cos\theta_{\mathrm{T}}$ was used to classify events as forward, with $y > 0$, or backward, with $y < 0$. The observed forward-backward asymmetry was then examined in bins of NETb, NETc and $|y|$. The fit considers four classes of leptons according to the lepton charge and primary quark flavour:

1. $\mathrm{b} \to \ell^-$, $\mathrm{b} \to \tau^- \to \ell^-$ and $\mathrm{b} \to \overline{\mathrm{c}} \to \ell^-$

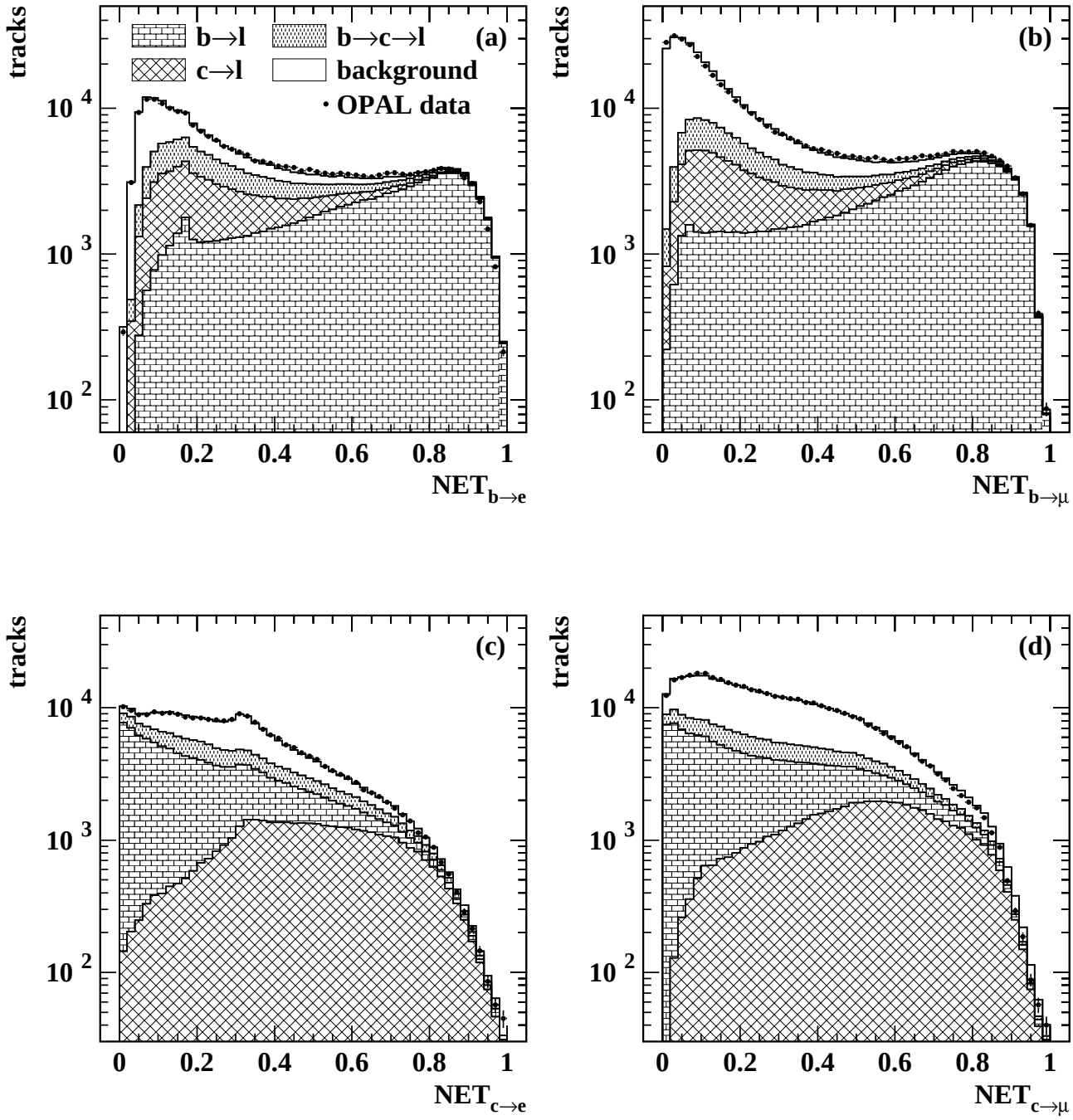

Figure 1: Outputs of the neural networks designed to select (a) b → e, (b) b → μ, (c) c → e and (d) c → μ decays. The data are shown by the points with error bars, and the expected contributions from different lepton sources by the hatched histograms.

2. $b \to c \to \ell^+$

3. $c \to \ell^+$

4. background

Direct $b \to \ell^-$ decays and the other decays in class (1) contribute to the observed asymmetry with the opposite sign to classes (2) and (3). The asymmetry of events coming from b decays is scaled by a factor $(1 - 2\overline{\chi})$ for category (1) decays, and $(1 - 2\overline{\eta}\,\overline{\chi})$ for category (2), to account for the effects of neutral B meson mixing. The additional correction factor $\overline{\eta}$ takes into account that the two samples include different fractions of different species of b hadron: B^0, B^+, B_s^0, b-baryons etc., due mainly to the different semileptonic branching ratios of D^0 and D^+ mesons. The value of $\overline{\eta}$ is set to 1.083, evaluated from the Monte Carlo simulation. No equivalent correction factor was used for the small fraction of $b \to \overline{c} \to \ell^-$ events included in category (1). The fractions of each single lepton category in the full data sample are given in Table 2. Note that these are fitted fractions. The fit adjusts the overall rate of background in the sample.

		electrons	muons
(1)	$b \to \ell^-$	35.6 %	24.6 %
	$b \to \overline{c} \to \ell^-$	2.8 %	2.3 %
	$b \to \tau^- \to \ell^-$	1.1 %	0.7 %
(2)	$b \to c \to \ell^+$	12.6 %	9.7 %
(3)	$c \to \ell^+$	19.3 %	14.9 %
(4)	background	28.6 %	47.8 %

Table 2: The composition of the single lepton samples. The first three lines are combined into category (1) in the fit. The fractions given correspond to the fractions f_i' after the fit.

	ee	$\mu\mu$	eμ
(1)(1)	86.9 %	86.3 %	86.4 %
(1)(2)	10.3 %	8.5 %	9.6 %
(2)(2)	0.3 %	0.2 %	0.3 %
(3)(3)	0.4 %	0.4 %	0.5 %
(1)(4)	1.8 %	4.0 %	2.8 %
others	0.3 %	0.6 %	0.4 %
total number	1 308	2 067	3 354

Table 3: Fractions of events in the most important categories in the double lepton sample, together with the total number of ee, $\mu\mu$ and eμ events.

The likelihood for single-lepton events has two terms:

$$\begin{aligned} \mathcal{L}_{\text{single }\ell} &= \prod_{\text{NETb,NETc}} \prod_{|y|} \frac{(n_\text{F}+n_\text{B})!}{n_\text{F}!\,n_\text{B}!} \left(\frac{1+A_\text{FB}}{2}\right)^{n_\text{F}} \left(\frac{1-A_\text{FB}}{2}\right)^{n_\text{B}} \\ &\times \prod_{\text{NETb,NETc}} \frac{1}{\sqrt{2\pi}\sigma_m} \exp\left(-\frac{(n_\text{T}-m)^2}{2\sigma_m^2}\right). \end{aligned} \tag{5}$$

The first term is a product over bins of NETb, NETc and $|y|$ of binomial probabilities for the number of forward and backward events observed in the data in each bin, n_F and n_B, depending on the asymmetry A_FB expected in the bin. The fit used 10 equally spaced bins in each of NETb, NETc and

	$A_{\rm FB}$ (%) (ZFITTER prediction)		
$\langle\sqrt{s}\rangle$ (GeV)	89.51	91.25	92.95
$s\bar{s}$	5.95± 5.0	9.64±1.3	11.89± 5.0
$u\bar{u}$	-3.08±20.0	6.32±7.3	12.07±20.0
$d\bar{d}$	5.96±10.0	9.64±3.7	11.89±10.0

Table 4: The values of the forward-backward asymmetries for light flavours taken from ZFITTER, and the variations used for calculating the background asymmetry.

	electrons		muons	
	$f^{q\bar{q}}_{\rm back}$	$c^{q\bar{q}}_{\rm dilute}$	$f^{q\bar{q}}_{\rm back}$	$c^{q\bar{q}}_{\rm dilute}$
$b\bar{b}$	0.139	0.028	0.192	0.093
$c\bar{c}$	0.146	-0.104	0.178	-0.043
$s\bar{s}$	0.214	0.025	0.243	0.103
$u\bar{u}$	0.220	-0.114	0.169	-0.123
$d\bar{d}$	0.218	0.107	0.218	0.083

Table 5: The fractions of background coming from each primary quark flavour for electrons and muons, and the dilution factors by which the primary quark forward-backward asymmetry are scaled to evaluate the background asymmetry.

$|y|$. The second term constrains the total number of events $n_{\rm T}$ in a given NETb-NETc bin (with no binning in $|y|$) to the expected number, m, and allowed the overall normalisations of the electron and muon backgrounds to be determined from the data, reducing the overall uncertainty.

The probability for an event to be forward is $(1 + A_{\rm FB})/2$ where $A_{\rm FB}$ is the expected forward-backward asymmetry in the bin considered:

$$A_{\rm FB}(\mathrm{NETb},\mathrm{NETc},|y|) = \sum_{i=1}^{4} f'_i \rho_i(\mathrm{NETb},\mathrm{NETc},|y|) A^i_{\rm FB}\ \frac{8}{3}\frac{|y|}{1+y^2}\,. \tag{6}$$

In this expression, f'_i denotes the fraction of leptons in class i, and ρ_i the normalised distribution of leptons from this class in bins of NETb, NETc and $|y|$, which is taken from Monte Carlo simulation. The source fractions f'_i are derived from the Monte Carlo fractions f_i. However, the fraction of background f'_4 is a free parameter in the fit, and the fractions of prompt sources with $i = 1, 2, 3$ are given by $f'_i = (1 - f'_4) f_i/(f_1 + f_2 + f_3)$. In this way, the relative rates of the prompt leptons are fixed by the Monte Carlo simulation, and the fractions satisfy $\sum_i f'_i = 1$. The nominal asymmetries $A^i_{\rm FB}$ for each class are:

$$\begin{array}{rcrl} A^1_{\rm FB} & = & & (1-2\overline{\chi})A^{b\bar{b}}_{\rm FB} \\ A^2_{\rm FB} & = & - & (1-2\overline{\eta}\,\overline{\chi})A^{b\bar{b}}_{\rm FB} \\ A^3_{\rm FB} & = & - & A^{c\bar{c}}_{\rm FB} \\ A^4_{\rm FB} & = & & A^{\rm Background}_{\rm FB} \end{array} \tag{7}$$

The background asymmetry $A^{\rm Background}_{\rm FB}$ also depends on the primary quark asymmetries. It is expressed as a sum over quark flavours:

$$A^{\rm Background}_{\rm FB} = \sum_{\rm q} f^{q\bar{q}}_{\rm back} c^{q\bar{q}}_{\rm dilute} A^{q\bar{q}}_{\rm FB}\,. \tag{8}$$

This introduces a very weak additional dependence on the fitted values of the b and c asymmetries. The central values of the light quark asymmetries are taken from the predictions of ZFITTER 6.36 [28], and are listed in Table 4. The quoted uncertainties in these asymmetries are taken from measurements

of the strange quark asymmetry by DELPHI [29] and of the light quark asymmetries by OPAL [30]. These measurements are consistent with the ZFITTER expectations, with relatively large statistical errors. The fractions $f_{\rm back}^{\rm q\overline{q}}$ of each quark flavour contributing to the background are taken from the Monte Carlo prediction, as are the dilution factors $c_{\rm dilute}^{\rm q\overline{q}}$ which take into account the fraction of the primary quark asymmetry that is seen in background events of this flavour. The fractions and dilutions are listed in Table 5. Some contributions to the background, for example for photon conversions, have zero forward-backward asymmetry. Others, in particular kaons in $\rm s\overline{s}$ events, inherit a significant fraction of the primary quark asymmetry. The background asymmetry actually varies as a function of NETb and NETc, but this effect is neglected in the fit as discussed in Section 5.3 below.

In the second term in the single lepton likelihood, the number of events, m, expected in a bin of NETb and NETc is calculated by:

$$m(\mathrm{NETb},\mathrm{NETc}) = N_{\rm Data}^{\ell} \sum_{i=1}^{4} f_i' \overline{\rho_i}(\mathrm{NETb},\mathrm{NETc})\,, \tag{9}$$

where $N_{\rm Data}^{\ell}$ denotes the total number of single lepton events in the data ($\ell = e,\ \mu$), and $\overline{\rho_i}$ is the normalised distribution in bins of NETb and NETc for leptons in class i. The observed number of events in a bin, $n_{\rm T}$, is assumed to be Gaussian distributed with mean m and standard deviation σ_m computed as $\sigma_m^2 = m + (\delta_m^{\rm MC})^2$, where $\delta_m^{\rm MC}$ is the uncertainty on the expected number m of events in this bin due to the limited Monte Carlo statistics.

4.2 Double lepton likelihood

The double lepton likelihood is a product in bins of $|y|$ of multinomial probabilities for the event to be forward, $p_{\rm F}$, backward, $p_{\rm B}$, or same-sign, $p_{\rm S}$. Both leptons have NETb > 0.6, and no further subdivision in NETb or NETc is made. The composition of the double lepton sample is given in Table 3. The ee, eμ and $\mu\mu$ events are all considered together:

$$\mathcal{L}_{\rm double} = \prod_{|y|} \frac{(n_{\rm F}+n_{\rm B}+n_{\rm S})!}{n_{\rm F}!\,n_{\rm B}!\,n_{\rm S}!}\ (p_{\rm F})^{n_{\rm F}}\ (p_{\rm B})^{n_{\rm B}}\ (p_{\rm S})^{n_{\rm S}}\ . \tag{10}$$

In this case, $n_{\rm F}$, $n_{\rm B}$ and $n_{\rm S}$ are the number of forward, backward and same-sign events observed in the data in this $|y|$ bin. A dilepton event with opposite charge leptons is called forward or backward according to the direction of the negative lepton. The probability of such an event being forward or backward usually depends on the forward-backward asymmetry of the dilepton category, ij, where the two indices refer to the categories $i = 1-4$ of the two leptons. The fraction of same-sign dilepton events depends only on the mixing parameter $\overline{\chi}$, and not on the asymmetries. Note that the fraction of forward and backward events with one lepton from category 1 and the other from category 2 is also independent of the forward-backward asymmetry, and only depends on the mixing parameter. This is because in the absence of mixing these events would all be same sign, losing the information about the asymmetry. If they are of opposite sign, without knowing which lepton comes from the mixed meson, the asymmetry information cannot be recovered.

Only certain categories ij are possible. Any flavour event can give a background lepton, but lepton classes 1 and 2 can only come from $\rm b\overline{b}$ events, and class 3 only from $\rm c\overline{c}$ events. The possible dilepton classes are therefore: $ij = 11, 12, 22, 33, 14, 24, 34, 44$. The overall probabilities for forward, backward or same sign events are given by a sum over the possible classes ij:

$$p_X = \sum_{ij} f_{ij}(|y|)\, p_X^{ij}(|y|) \tag{11}$$

Since the contribution of background leptons to the double-lepton sample is small (see Table 3), the fractions f_{ij} are taken directly from the Monte Carlo simulation, without being corrected for the rates

of background leptons fitted in the single lepton sample. Similarly, the small residual asymmetries of the background leptons are neglected. Writing $Y = 8|y|/3(1+y^2)$, the probabilities $p^{ij}_{\mathrm{F,B,S}}$ for an event to be forward, backward or same-sign for each dilepton category are given by:

$$
\begin{aligned}
p_{\mathrm{F}}^{11} &= \tfrac{1}{2}(1 - 2\overline{\chi} + 2\overline{\chi}^2 + (1-2\overline{\chi})A_{\mathrm{FB}}^{\mathrm{b\overline{b}}}Y) \\
p_{\mathrm{B}}^{11} &= \tfrac{1}{2}(1 - 2\overline{\chi} + 2\overline{\chi}^2 - (1-2\overline{\chi})A_{\mathrm{FB}}^{\mathrm{b\overline{b}}}Y) \\
p_{\mathrm{S}}^{11} &= 2\overline{\chi}(1-\overline{\chi}) \\
p_{\mathrm{F}}^{12} &= \tfrac{1}{2}\overline{\eta}\,\overline{\chi}(1-\overline{\chi}) + \tfrac{1}{2}\overline{\chi}(1-\overline{\eta}\,\overline{\chi}) \\
p_{\mathrm{B}}^{12} &= \tfrac{1}{2}\overline{\eta}\,\overline{\chi}(1-\overline{\chi}) + \tfrac{1}{2}\overline{\chi}(1-\overline{\eta}\,\overline{\chi}) \\
p_{\mathrm{S}}^{12} &= (1-\overline{\chi})(1-\overline{\eta}\,\overline{\chi}) + \overline{\eta}\,\overline{\chi}^2 \\
p_{\mathrm{F}}^{22} &= \tfrac{1}{2}(1 - 2\overline{\eta}\,\overline{\chi} + 2(\overline{\eta}\,\overline{\chi})^2 - (1-2\overline{\eta}\,\overline{\chi})A_{\mathrm{FB}}^{\mathrm{b\overline{b}}}Y) \\
p_{\mathrm{B}}^{22} &= \tfrac{1}{2}(1 - 2\overline{\eta}\,\overline{\chi} + 2(\overline{\eta}\,\overline{\chi})^2 + (1-2\overline{\eta}\,\overline{\chi})A_{\mathrm{FB}}^{\mathrm{b\overline{b}}}Y) \\
p_{\mathrm{S}}^{22} &= 2\overline{\eta}\,\overline{\chi}(1-\overline{\eta}\,\overline{\chi}) \\
p_{\mathrm{F}}^{33} &= \tfrac{1}{2}(1 - A_{\mathrm{FB}}^{\mathrm{c\overline{c}}}Y) \\
p_{\mathrm{B}}^{33} &= \tfrac{1}{2}(1 + A_{\mathrm{FB}}^{\mathrm{c\overline{c}}}Y) \\
p_{\mathrm{S}}^{33} &= 0 \\
p_{\mathrm{F}}^{14} &= \tfrac{1}{4}(1-\overline{\chi})(1 + A_{\mathrm{FB}}^{\mathrm{b\overline{b}}}Y) + \tfrac{1}{4}\overline{\chi}(1 - A_{\mathrm{FB}}^{\mathrm{b\overline{b}}}Y) \\
p_{\mathrm{B}}^{14} &= \tfrac{1}{4}(1-\overline{\chi})(1 - A_{\mathrm{FB}}^{\mathrm{b\overline{b}}}Y) + \tfrac{1}{4}\overline{\chi}(1 + A_{\mathrm{FB}}^{\mathrm{b\overline{b}}}Y) \\
p_{\mathrm{S}}^{14} &= \tfrac{1}{2} \\
p_{\mathrm{F}}^{24} &= \tfrac{1}{4}(1-\overline{\eta}\,\overline{\chi})(1 - A_{\mathrm{FB}}^{\mathrm{b\overline{b}}}Y) + \tfrac{1}{4}\overline{\eta}\,\overline{\chi}(1 + A_{\mathrm{FB}}^{\mathrm{b\overline{b}}}Y) \\
p_{\mathrm{B}}^{24} &= \tfrac{1}{4}(1-\overline{\eta}\,\overline{\chi})(1 + A_{\mathrm{FB}}^{\mathrm{b\overline{b}}}Y) + \tfrac{1}{4}\overline{\eta}\,\overline{\chi}(1 - A_{\mathrm{FB}}^{\mathrm{b\overline{b}}}Y) \\
p_{\mathrm{S}}^{24} &= \tfrac{1}{2} \\
p_{\mathrm{F}}^{34} &= \tfrac{1}{4}(1 - A_{\mathrm{FB}}^{\mathrm{c\overline{c}}}Y) \\
p_{\mathrm{B}}^{34} &= \tfrac{1}{4}(1 + A_{\mathrm{FB}}^{\mathrm{c\overline{c}}}Y) \\
p_{\mathrm{S}}^{34} &= \tfrac{1}{2} \\
p_{\mathrm{F}}^{44} &= \tfrac{1}{4} \\
p_{\mathrm{B}}^{44} &= \tfrac{1}{4} \\
p_{\mathrm{S}}^{44} &= \tfrac{1}{2}
\end{aligned}
\tag{12}
$$

4.3 Results

The data are divided into three separate energy bins whose mean energies are shown in Table 1. The asymmetries were fitted simultaneously at all energy points, the overall likelihood being the product of the likelihood in Equation 4 for each point. Therefore, the fit has nine free parameters: the asymmetries $A_{\mathrm{FB}}^{\mathrm{b\overline{b}}}$ and $A_{\mathrm{FB}}^{\mathrm{c\overline{c}}}$ at three energy points, together with values common to all three energy points for the mixing parameter $\overline{\chi}$, and the electron and muon background fractions, f_4'. Data from all years were fitted simultaneously, with the various fractions and (NETb, NETc) distributions determined from an appropriate mix of Monte Carlo events with different simulated detector configurations, taking into account the changes in the performance of the OPAL detector over time.

The result of the fit is illustrated in Figure 2. For this plot, two regions of NETb-NETc were selected, one 93 % pure in $\mathrm{b} \to \ell^-$ events and the other 59 % pure in $\mathrm{c} \to \ell^+$ events. The asymmetry observed in the data in bins of $|y|$ and the predicted asymmetry according to Equation 6 are shown. The predicted asymmetry is calculated with the fitted results. The sign of the observed asymmetry is clearly different in the two regions.

A small correction is applied to the fitted asymmetries to correct for the effects of gluon radiation from the primary quark pair and the approximation of the original quark direction by the experimentally measured thrust axis [31]. The effects of gluon radiation have been calculated to second order in α_s using the parton level thrust axis to define the asymmetry [32], and the translation from the parton level to the hadron level thrust axis (defined using all final state particles without detector effects) has been determined using Monte Carlo hadronisation models [31]. However, the detector acceptance and fitting method introduce additional biases which reduce the sensitivity of the analysis to these QCD corrections. Therefore, the final correction applied to the fitted asymmetries is determined by comparing the asymmetries fitted on large samples of Monte Carlo simulated events with the true quark level asymmetries, after scaling the hadron level thrust axis QCD corrections in the Monte Carlo to the theoretical values [33]. This procedure also accounts for any other residual biases in the fit, for example from the treatment of the background asymmetry. Combining all effects, the raw fitted asymmetries were scaled by factors of $1.0050 \pm 0.0063 \pm 0.0050$ for b quarks and $1.0117 \pm 0.0063 \pm 0.0062$ for c quarks to determine the quark level results, where the first errors result from theoretical uncertainties [31, 33] and the second from limited Monte Carlo statistics.

After correcting for QCD effects, the results are:

$$\begin{aligned}
A_{\rm FB}^{\rm b\overline{b}} &= (\ 4.7\ \pm 1.8\ \pm 0.1\ )\,\% \quad A_{\rm FB}^{\rm c\overline{c}} = (-6.8\ \pm 2.5\ \pm 0.9\ )\,\% \quad \text{at } \langle\sqrt{s}\rangle = 89.51 \text{ GeV},\\
A_{\rm FB}^{\rm b\overline{b}} &= (\ 9.72 \pm 0.42 \pm 0.15)\,\% \quad A_{\rm FB}^{\rm c\overline{c}} = (\ 5.68 \pm 0.54 \pm 0.39)\,\% \quad \text{at } \langle\sqrt{s}\rangle = 91.25 \text{ GeV},\\
A_{\rm FB}^{\rm b\overline{b}} &= (10.3\ \pm 1.5\ \pm 0.2\ )\,\% \quad A_{\rm FB}^{\rm c\overline{c}} = (\ 14.6\ \pm 2.0\ \pm 0.8\ )\,\% \quad \text{at } \langle\sqrt{s}\rangle = 92.95 \text{ GeV}.
\end{aligned}$$

For the average B mixing parameter, a value of:

$$\overline{\chi} = (13.12 \pm 0.49 \pm 0.42)\,\%$$

is obtained. In each case the first error is statistical and the second systematic. The evaluation of the systematic errors is described in the following section. The statistical correlations between the results are given in Table 6. The background levels in the electron and muon samples were fitted to be (89.4 ± 0.6) % and (94.4 ± 0.3) % of the rates estimated from Monte Carlo simulation, where the quoted errors are statistical only. These values are consistent with the known uncertainties in modelling the lepton background levels [17].

peak	$A_{\rm FB}^{\rm b\overline{b}}$	$A_{\rm FB}^{\rm c\overline{c}}$	$\overline{\chi}$
$A_{\rm FB}^{\rm b\overline{b}}$	1.00	0.17	0.30
$A_{\rm FB}^{\rm c\overline{c}}$		1.00	0.01
$\overline{\chi}$			1.00

peak−2	$A_{\rm FB}^{\rm b\overline{b}}$	$A_{\rm FB}^{\rm c\overline{c}}$	$\overline{\chi}$
$A_{\rm FB}^{\rm b\overline{b}}$	1.00	0.18	0.03
$A_{\rm FB}^{\rm c\overline{c}}$		1.00	0.00
$\overline{\chi}$			1.00

peak+2	$A_{\rm FB}^{\rm b\overline{b}}$	$A_{\rm FB}^{\rm c\overline{c}}$	$\overline{\chi}$
$A_{\rm FB}^{\rm b\overline{b}}$	1.00	0.17	0.10
$A_{\rm FB}^{\rm c\overline{c}}$		1.00	0.00
$\overline{\chi}$			1.00

Table 6: Statistical correlation matrices at each centre-of-mass energy using the entire (1990–2000) data sample. The correlations with the fitted background fractions are negligibly small (< 0.01) and are not given here.

5 Systematic uncertainties

Systematic uncertainties result from a number of sources, including modelling of b and c hadron production and decay, external branching ratio inputs, background uncertainties and the performance of the OPAL detector. For the first two sources, the proposals of the LEP Heavy Flavour Electroweak Working Group have been adopted [33]. Where errors are only assessed by a variation in one direction, for example to an alternative model, or when slightly asymmetric errors are assessed, the larger deviation is taken as 1σ. The systematic errors are summarised in Tables 7 and 8 and discussed in more detail below. The signs of the errors indicate the direction of change in the result when the corresponding quantity is varied.

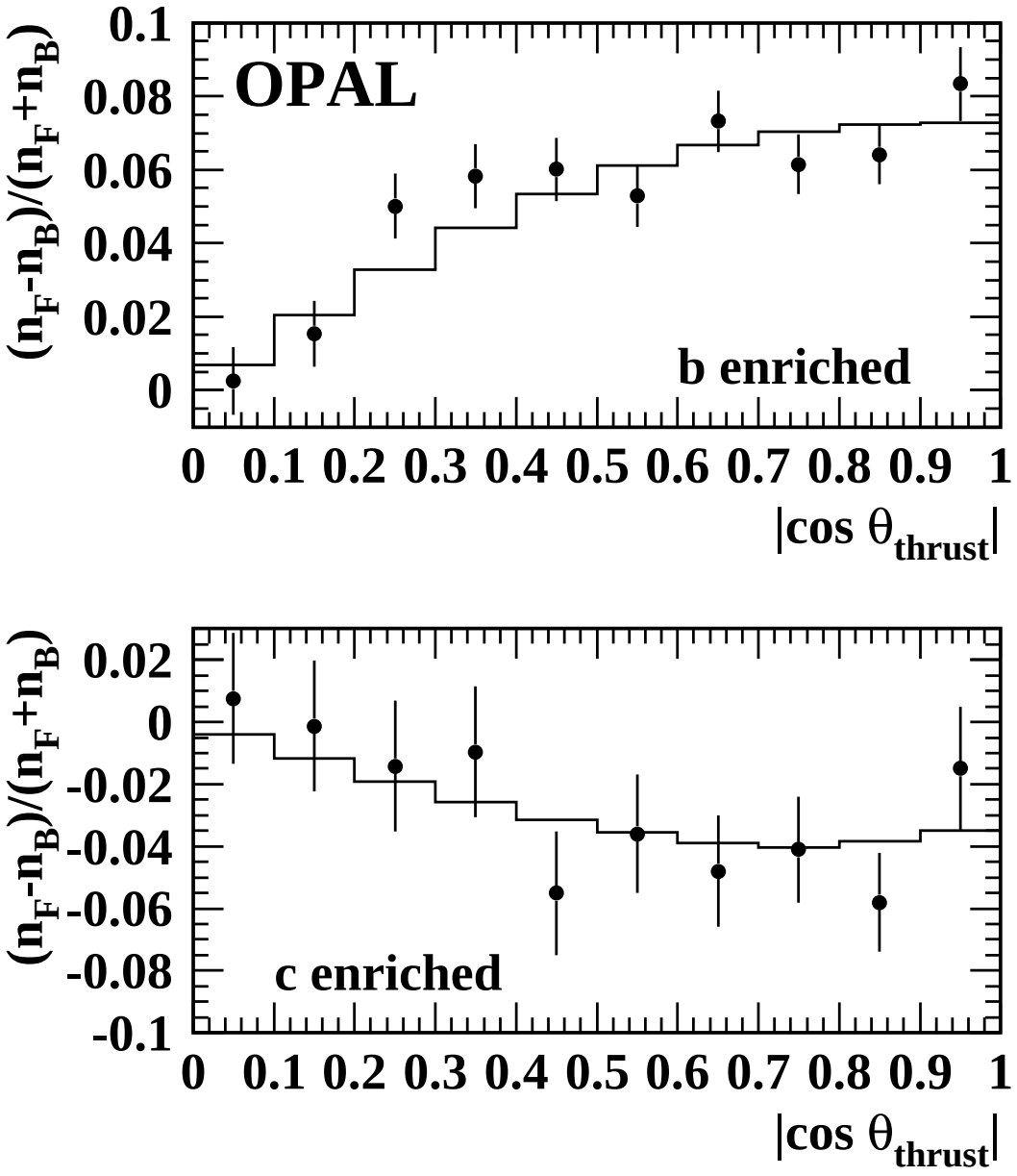

Figure 2: An illustration of the fit results for (a) a b enriched region and (b) a c enriched region of NETb-NETc space. The asymmetry observed in the data in each bin of $|y|$ is compared with the expectation calculated from the full fit. The errors are purely statistical.

	$A_{\rm FB}^{\rm b\overline{b}}(\%)$	$A_{\rm FB}^{\rm c\overline{c}}(\%)$	$\overline{\chi}(\%)$
Fitted Value	9.716	5.683	13.121
Statistical error	$\pm$0.418	$\pm$0.542	$\pm$0.485
Systematic error	$\pm$0.150	$\pm$0.386	$\pm$0.421
Sources of systematic errors			
$b \to \ell^-$ semileptonic decay model	$\pm$0.011	$\mp$0.101	$\pm$0.175
$c \to \ell^+$ semileptonic decay model	$\pm$0.064	$\mp$0.036	$\mp$0.286
$\langle x_E^{\rm b} \rangle$ $\pm$0.008	$\mp$0.012	$\mp$0.008	$\mp$0.074
$\langle x_E^{\rm c} \rangle$ $\pm$0.008	$\pm$0.054	$\mp$0.024	$\pm$0.010
Total models	0.085	0.110	0.344
BR($b \to \ell^-$) (10.65 $\pm$0.23) %	$\mp$0.020	$\pm$0.104	$\pm$0.120
BR($b \to c \to \ell^+$) (8.08$\pm$0.18) %	$\mp$0.006	$\mp$0.050	$\mp$0.105
BR($b \to \overline{c} \to \ell^-$) (1.62$\pm$0.44) %	$\pm$0.011	$\pm$0.174	$\pm$0.014
BR($b \to \tau^- \to \ell^-$) (0.419$\pm$0.05) %	$\mp$0.001	$\pm$0.028	$\pm$0.007
BR($c \to \ell^+$) (9.77$\pm$0.32) %	$\pm$0.028	$\mp$0.151	$\pm$0.008
$R_{\rm b}$ (21.647$\pm$0.072) %	$\mp$0.003	$\pm$0.009	0.000
$R_{\rm c}$ (16.83$\pm$0.47) %	$\pm$0.019	$\mp$0.099	$\pm$0.002
Total branching ratios	0.041	0.277	0.161
e ID efficiency $\pm$ 4.1 %	$\mp$0.005	$\mp$0.007	$\pm$0.004
μ ID efficiency $\pm$ 3.0 %	$\mp$0.002	$\mp$0.021	$\pm$0.022
Conversions $\pm$15 %	$\pm$0.001	$\pm$0.012	$\mp$0.007
Muon background (K) $\pm$30 %	$\pm$0.011	$\pm$0.023	$\mp$0.034
Muon background (π) $\pm$5 %	$\pm$0.004	$\pm$0.026	$\mp$0.015
Muon background (other) $\pm$100 %	$\pm$0.009	$\pm$0.017	$\mp$0.058
Background asymmetry u,d,s events	$\pm$0.002	$\pm$0.102	$\pm$0.002
Background flavour separation	$\pm$0.020	$\pm$0.020	0.000
Total background effects	0.026	0.114	0.073
Correction of $\bar{\chi}$ for $b \to c \to \ell^+$	$-$0.008	$-$0.069	$-$0.068
$\cos\theta_{\rm T}$ dependence (fractions)	$-$0.018	+0.001	+0.000
Tracking resolution	$-$0.025	$-$0.046	$-$0.016
Flavour separation variables	$\pm$0.067	$\pm$0.163	$\pm$0.099
Time dependent mixing	+0.032	+0.098	$-$0.091
Monte Carlo statistics	$\pm$0.050	$\pm$0.041	$\pm$0.070
Charge reconstruction	$\pm$0.015	$\pm$0.004	0.000
LEP centre-of-mass energy	$\pm$0.010	$\pm$0.027	0.000
QCD correction	$\pm$0.061	$\pm$0.036	0.000
Total other systematics	0.114	0.216	0.167

Table 7: Results and breakdown of systematic uncertainties for the on-peak forward-backward asymmetries and the mixing parameter $\overline{\chi}$.

	Peak–2		**Peak+2**	
	$A_{\rm FB}^{\rm b\bar{b}}(\%)$	$A_{\rm FB}^{\rm c\bar{c}}(\%)$	$A_{\rm FB}^{\rm b\bar{b}}(\%)$	$A_{\rm FB}^{\rm c\bar{c}}(\%)$
Fitted Value	4.70	-6.83	10.31	14.59
Statistical error	$\pm$1.80	$\pm$2.52	$\pm$1.50	$\pm$2.04
Systematic error	$\pm$0.098	$\pm$0.928	$\pm$0.224	$\pm$0.837
Sources of systematic errors				
$b \to \ell^-$ semileptonic decay model	$\pm$0.031	$\mp$0.036	$\mp$0.020	$\mp$0.101
$c \to \ell^+$ semileptonic decay model	$\mp$0.019	$\pm$0.070	$\pm$0.106	$\mp$0.108
$\langle x_E^{\rm b} \rangle$ $\pm$0.008	$\mp$0.008	$\mp$0.037	$\mp$0.019	$\mp$0.034
$\langle x_E^{\rm c} \rangle$ $\pm$0.008	$\mp$0.013	$\pm$0.009	$\pm$0.090	$\mp$0.051
Total models	0.039	0.088	0.142	0.160
BR($b \to \ell^-$) (10.65 $\pm$0.23) %	$\mp$0.001	$\mp$0.034	$\mp$0.012	$\pm$0.198
BR($b \to c \to \ell^+$) (8.08$\pm$0.18) %	$\mp$0.003	$\mp$0.047	$\mp$0.024	$\mp$0.036
BR($b \to \overline{c} \to \ell^-$) (1.62$\pm$0.44) %	$\mp$0.023	$\pm$0.024	$\pm$0.055	$\pm$0.250
BR($b \to \tau^- \to \ell^-$) (0.419$\pm$0.05) %	$\mp$0.003	$\mp$0.002	$\mp$0.002	$\pm$0.044
BR($c \to \ell^+$) (9.77$\pm$0.32) %	$\pm$0.009	$\pm$0.161	$\pm$0.033	$\mp$0.381
$R_{\rm b}$ (21.647$\pm$0.072) %	$\mp$0.001	$\mp$0.010	$\mp$0.004	$\pm$0.023
$R_{\rm c}$ (16.83$\pm$0.47) %	$\pm$0.006	$\pm$0.106	$\pm$0.023	$\mp$0.250
Total branching ratios	0.026	0.203	0.074	0.560
e ID efficiency $\pm$ 4.1 %	$\mp$0.001	$\pm$0.005	$\mp$0.007	$\mp$0.019
μ ID efficiency $\pm$ 3.0 %	$\mp$0.002	$\pm$0.030	$\mp$0.002	$\mp$0.049
Conversions $\pm$15 %	$\pm$0.003	$\mp$0.002	$\pm$0.003	$\pm$0.025
Muon background (K) $\pm$30 %	$\pm$0.003	$\mp$0.032	$\pm$0.010	$\pm$0.073
Muon background (π) $\pm$5 %	$\pm$0.003	$\mp$0.036	$\pm$0.005	$\pm$0.056
Muon background (other) $\pm$100 %	$\pm$0.002	$\mp$0.044	$\pm$0.009	$\pm$0.062
Background asymmetry u,d,s events	$\pm$0.018	$\pm$0.832	$\pm$0.006	$\pm$0.302
Background flavour separation	$\pm$0.020	$\pm$0.025	$\pm$0.010	$\pm$0.065
Total background effects	0.028	0.836	0.021	0.333
Correction of $\bar{\chi}$ for $b \to c \to \ell^+$	$-$0.000	$-$0.033	$-$0.027	$-$0.079
$\cos\theta_{\rm T}$ dependence (fractions)	+0.005	$-$0.024	$-$0.030	+0.001
Tracking resolution	$-$0.011	+0.261	$-$0.002	$-$0.215
Flavour separation variables	$\pm$0.029	$\pm$0.172	$\pm$0.097	$\pm$0.403
Time dependent mixing	$-$0.037	+ 0.036	+0.069	+0.112
Monte Carlo statistics	$\pm$0.058	$\pm$0.102	$\pm$0.064	$\pm$0.118
Charge reconstruction	$\pm$0.007	$\pm$0.005	$\pm$0.016	$\pm$0.010
LEP centre-of-mass energy	$\pm$0.007	$\pm$0.018	$\pm$0.003	$\pm$0.007
QCD correction	$\pm$0.030	$\pm$0.043	$\pm$0.062	$\pm$0.092
Total other systematics	0.082	0.337	0.155	0.500

Table 8: Results and breakdown of systematic uncertainties for the off-peak forward-backward asymmetries.

5.1 Modelling of b and c production and decay

Semileptonic decay models: A correct description of the lepton momentum spectra in the rest frame of decaying b and c hadrons is crucial for the flavour separation. The semileptonic decays of heavy hadrons were described by the free-quark model of Altarelli *et al.* (ACCMM) [21], with its two free parameters fixed by fits to CLEO data [22] for $b \to \ell^-$ decays and the combined measurements of DELCO [23] and MARK III [24] for $c \to \ell^+$ decays [33]. For cascade decays $b \to c \to \ell^+$ and $b \to \overline{c} \to \ell^-$, the D momentum spectrum measured by CLEO [35] is combined with the $c \to \ell^+$ model to generate the lepton momentum distribution. Uncertainties in the CLEO D momentum spectrum are negligible compared with the uncertainties in the $b \to \ell^-$ and $c \to \ell^+$ models.

For $b \to \ell^-$ decays, the systematic uncertainties were assessed by reweighting the rest frame momentum spectrum according to the form-factor model of Isgur *et al.* [34], which has no free parameters (ISGW). This spectrum is harder than the central ACCMM model. As an alternative, the same model was used with the fraction of D^{**} mesons produced in b decays increased from 11 % to 32 % to describe better CLEO data, denoted ISGW**. This gives a softer spectrum than the default model. Although the weights to go from model to model were evaluated using only B^0 and B^+ meson decays, these weights were then applied to all b-hadron decays. Variations in the $c \to \ell^+$ decay model were assessed by varying the free parameters of the ACCMM model to give harder or softer decay models, constrained by the DELCO and MARK III data. For both $b \to \ell^-$ and $c \to \ell^+$ decays, the sign of the error assigned indicates the variation observed with the harder alternative spectrum.

Heavy quark fragmentation: The lepton momentum spectra depend on the energy distributions of the heavy hadrons produced in $b\overline{b}$ and $c\overline{c}$ events. The Monte Carlo events were reweighted so as to vary the average scaled energy $\langle x_E \rangle$ of weakly decaying b hadrons in the range $\langle x_E \rangle = 0.702 \pm 0.008$ and of c hadrons in the range $\langle x_E \rangle = 0.484 \pm 0.008$ [33]. The fragmentation functions of Peterson *et al.*, Collins and Spiller, Kartvelishvili *et al.* and the Lund group [20, 36] were each used as models to determine the event weights, and the largest observed variations were assigned as the systematic errors. For b fragmentation, the largest shifts were observed with the function of Collins and Spiller, and for c fragmentation with the function of Peterson *et al.*

5.2 Branching ratios and partial widths

Semileptonic branching ratios: The values and uncertainties used for the branching ratios of semileptonic b and c hadron decays are listed in Tables 7 and 8 [2, 33].

Partial widths of the Z: The fractions of hadronic Z decays to $b\overline{b}$ and $c\overline{c}$ were varied according to the uncertainties in the LEP average values [2]: $R_b = 0.21647 \pm 0.00072$ and $R_c = 0.1683 \pm 0.0047$. In each case, the fraction of Z hadronic decays to light quarks was adjusted to compensate the variation.

5.3 Background uncertainties

Lepton identification: The analysis is only weakly sensitive to the lepton identification efficiency, since this mainly affects the ratio of prompt to background leptons, which is effectively determined from the data via the fit of the background level. However, a small component of the background is composed of genuine leptons, so the lepton identification efficiencies were varied by ±4.1 % for electrons and ±3.0 % for muons [17].

Background composition: The overall background fraction is a fitted parameter. However, the background shape as a function of NETb, NETc and $|y|$ may be different for different contributions to the background. The rate of untagged photon conversions was varied by ±15 % [17]. In

addition, the $|y|$ distribution of conversions was varied according to the difference in the rate of identified conversions observed between data and Monte Carlo simulation. The contributions to the muon background from π, K and other sources were varied in turn by 5 %, 30 % and 100 %. These uncertainties were evaluated using control samples of $\mathrm{K}^0_\mathrm{s} \to \pi^+\pi^-$, three-prong tau decays and tracks with an enhanced kaon fraction selected using $\mathrm{d}E/\mathrm{d}x$ cuts [37]. The variation of the source fractions, including backgrounds, as a function of $\cos\theta_\mathrm{T}$ is discussed in Section 5.4 below.

Background asymmetries: The uncertainties in the background asymmetry were evaluated by varying the light primary quark forward-backward asymmetries by the uncertainties listed in Table 4. Note that the up and down asymmetries measured by OPAL are +91 % correlated [30]. They were therefore varied at the same time, and the resulting uncertainty combined in quadrature with the uncertainty in the strange asymmetry. The $\mathrm{b\overline{b}}$ and $\mathrm{c\overline{c}}$ asymmetries are treated self-consistently in the fit, and the uncertainty in these quantities is therefore automatically reflected in a very small contribution to the statistical uncertainty.

Background flavour separation: The dependence of the background asymmetry on NETb and NETc is neglected in the fit (see Equation 8) but any residual bias is removed by the bias correction as discussed in Section 4.3, providing the Monte Carlo gives an adequate description of the variations. To quantify the size of any mismodelling, an additional fit was performed using a binned background asymmetry without changing the bias correction, and half the difference between this and the standard fit result was assigned as a systematic error.

5.4 Other uncertainties

Correction factor for mixing in cascade decays: The difference between using the standard value of $\overline{\eta} = 1.083$ and setting it equal to 1.000 was assigned as a conservative estimate of the uncertainty.

Dependence of source fractions on $\cos\theta_\mathrm{T}$: The description of the source fractions as a function of $\cos\theta_\mathrm{T}$ was checked by selecting $\mathrm{b} \to \ell^-$, $\mathrm{c} \to \ell^+$ and background enriched regions of the NETb–NETc plane, and comparing the $\cos\theta_\mathrm{T}$ distributions of data and Monte Carlo simulation. No systematic trend was seen for the $\mathrm{c} \to \ell^+$ enriched sample. The ratio for background varied by up to 10 % in the endcap region, with smaller deviations for the $\mathrm{b} \to \ell^-$ enriched sample. A systematic uncertainty was therefore assessed by reweighting the Monte Carlo background according to the data/Monte Carlo ratio observed for the background enriched sample, and repeating the fit. The change in the background sample was compensated by an increase in the prompt leptons, so this procedure also accounted for any possible discrepancy in the $\mathrm{b} \to \ell^-$ sample.

Tracking resolution: A global 10 % degradation in the tracking resolution was applied to the Monte Carlo sample, separately in the r-ϕ and r-z planes, as discussed in [17, 10]. The fit was repeated with each of these modified samples, and the sum in quadrature of the two shifts in the results was taken as a systematic uncertainty.

Flavour separation variables: Possible uncertainties due to mismodelling of the neural network input variables were taken into account by reweighting the Monte Carlo events by the ratio between the data and Monte Carlo distributions of each variable in turn, and repeating the fit. The sum in quadrature of the shifts in the results was assigned as a systematic uncertainty, dominated by the result of reweighting the lepton p and p_t distributions for the asymmetries, and the input parameter significance for $\overline{\chi}$. The neural network output distributions were also reweighted, to account for the discrepancies between data and Monte Carlo visible in Figure 1, but the resulting changes in the results were much smaller than those seen when reweighting the inputs, and no additional systematic error was assigned.

Time dependent mixing: The mixing parameter $\overline{\chi}$ reflects the fraction of mixed events in an unbiased sample of all b hadrons. However, the time dependent oscillations for B^0 mesons are sufficiently slow that the lifetime variables used in NETc might change the effective value of $\overline{\chi}$ as a function of NETc. To evaluate the impact of such an effect, the value of $\overline{\chi}$ was evaluated for all $b\overline{b}$ Monte Carlo events with a lepton candidate, in bins of NETc, and for the entire $b\overline{b}$ sample. The fitted value of $\overline{\chi}$ in the likelihood function was then scaled by the ratio of Monte Carlo values of $\overline{\chi}$ in the NETc bin and $\overline{\chi}$ in all $b\overline{b}$ events. The shift in the fit results with this rescaling was taken as a systematic uncertainty.

Monte Carlo statistics: The fit to the data was repeated 1000 times, with the Monte Carlo reference distributions being randomly varied according to the statistical uncertainty in each bin of NETb, NETc and $|y|$. The RMS variation in the results was added in quadrature with the Monte Carlo statistical uncertainty on the bias corrections discussed in Section 4.3 to give the total uncertainty due to limited Monte Carlo statistics.

Lepton charge reconstruction and asymmetry: Monte Carlo simulation predicts that about 0.03 % of electrons and 0.3 % of muons are reconstructed in the tracking chamber with the wrong charge (electron tracks are subject to tighter quality requirements because of the stronger $\mathrm{d}E/\mathrm{d}x$ cuts). This effect is accounted for in the fit, and the full size of the correction is taken as a systematic error. Studies in [38] show a possible difference of around 10^{-3} between the lepton identification efficiencies for positive and negative tracks. When combined with the small difference (2 %) in numbers of reconstructed leptons in positive and negative hemispheres, this leads to negligible asymmetry biases of around 2×10^{-5}.

LEP centre-of-mass energy: The LEP centre of mass energy is known to a precision varying between 3.5 and 20 MeV depending on the energy point and year [39]. Taking year-to-year correlations into account, and assuming the Standard Model dependencies of the asymmetries on $\sqrt{s}$, this leads to the uncertainties given in Tables 7 and 8 on the asymmetries at the quoted values of $\sqrt{s}$.

QCD and thrust axis correction: The corrections applied to the raw fitted asymmetries are known to precisions of 0.80 % for b quarks and 0.89 % for c quarks, as discussed in Section 4. The theoretical part of this uncertainty is assigned as the error on the QCD correction, whilst the Monte Carlo statistical uncertainty is accounted for separately as discussed above.

5.5 Consistency checks

The analysis was performed separately for data from 1990 and 1991, for each year separately from 1992 to 1995, and for data from 1996 to 2000. The results were consistent among themselves and with the standard result from fitting all data simultaneously. Taking into account statistical errors only, the χ^2/dof value for the six $A_{\mathrm{FB}}^{\mathrm{b\overline{b}}}$ measurements to be consistent with the same value was 5.9/5. The equivalent χ^2/dof values for $A_{\mathrm{FB}}^{\mathrm{c\overline{c}}}$ and $\overline{\chi}$ were 2.4/5 and 5.3/5. Separate fits for electron and muon events were also made and showed similar consistency. The number of bins in y, NETb and NETc were varied, and again consistent results were obtained. To verify the correctness of the fit method itself, it was tested on large samples of test Monte Carlo samples generated with various b and c asymmetries and with source fractions and input NETb and NETc distributions generated to correspond to those in the full simulation. In these tests, the fit was found to be unbiased and to return correct statistical errors on the fitted parameters.

6 Conclusions

The forward-backward asymmetries of $e^+e^- \to b\overline{b}$ and $e^+e^- \to c\overline{c}$ events have been measured at three energy points around the Z peak, using electrons and muons produced in semileptonic decays of bottom and charm hadrons. The results, corrected to the primary quark level, are:

$$\begin{array}{ll}
A_{\rm FB}^{b\overline{b}} = (\ 4.7\ \pm 1.8\ \pm 0.1\ )\,\% & A_{\rm FB}^{c\overline{c}} = (-6.8\ \pm 2.5\ \pm 0.9\ )\,\% \quad \text{at } \langle\sqrt{s}\rangle = 89.51 \text{ GeV}, \\
A_{\rm FB}^{b\overline{b}} = (\ 9.72 \pm 0.42 \pm 0.15)\,\% & A_{\rm FB}^{c\overline{c}} = (\ 5.68 \pm 0.54 \pm 0.39)\,\% \quad \text{at } \langle\sqrt{s}\rangle = 91.25 \text{ GeV}, \\
A_{\rm FB}^{b\overline{b}} = (10.3\ \pm 1.5\ \pm 0.2\ )\,\% & A_{\rm FB}^{c\overline{c}} = (\ 14.6\ \pm 2.0\ \pm 0.8\ )\,\% \quad \text{at } \langle\sqrt{s}\rangle = 92.95 \text{ GeV}.
\end{array}$$

For the average B mixing parameter, a value of:

$$\overline{\chi} = (13.12 \pm 0.49 \pm 0.42)\,\%$$

is obtained. In each case the first error is statistical and the second systematic. The asymmetry results are shown as a function of $\sqrt{s}$ in Figure 3.

Using the ZFITTER prediction for the dependence of $A_{\rm FB}^{b\overline{b}}$ and $A_{\rm FB}^{c\overline{c}}$ on $\sqrt{s}$, the measurements are shifted to $m_{\rm Z}$ (91.19 GeV), averaged and corrected for initial state radiation, γ exchange, $\gamma - Z$ interference and quark mass effects. The results for the pole asymmetries are:

$$\begin{aligned}
A_{\rm FB}^{0,\,b} &= (9.81 \pm 0.40 \pm 0.15)\,\%\,, \\
A_{\rm FB}^{0,\,c} &= (6.29 \pm 0.52 \pm 0.38)\,\%\,.
\end{aligned}$$

These results are consistent with those of $A_{\rm FB}^{b\overline{b}}$ derived from inclusive jet charge measurements [10] and those of $A_{\rm FB}^{b\overline{b}}$ and $A_{\rm FB}^{c\overline{c}}$ derived from fully reconstructed charm hadrons [13]. Whilst the statistical correlations between the asymmetries measured here and those from reconstructed charm hadrons are negligible, the jet charges of some of the events involving $b \to \ell^-$ decays are also used to measure $A_{\rm FB}^{b\overline{b}}$ in [10]. This results in a statistical correlation of 0.11 ± 0.12 between the two measurements, evaluated using large samples of Monte Carlo simulated events. Taking both statistical and systematic correlations into account, and making very small corrections to the inclusive and charm meson asymmetries to use the same nominal centre-of-mass energies as in this analysis, the final OPAL results for the b and c quark asymmetries around the Z resonance are:

$$\begin{array}{ll}
A_{\rm FB}^{b\overline{b}} = (\ 5.3\ \pm 1.2\ \pm 0.1\ )\,\% & A_{\rm FB}^{c\overline{c}} = (-4.8\ \pm 2.2\ \pm 0.7\ )\,\% \quad \text{at } \langle\sqrt{s}\rangle = 89.51 \text{ GeV}, \\
A_{\rm FB}^{b\overline{b}} = (\ 9.69 \pm 0.29 \pm 0.13)\,\% & A_{\rm FB}^{c\overline{c}} = (\ 5.83 \pm 0.49 \pm 0.32)\,\% \quad \text{at } \langle\sqrt{s}\rangle = 91.25 \text{ GeV}, \\
A_{\rm FB}^{b\overline{b}} = (11.4\ \pm 1.0\ \pm 0.2\ )\,\% & A_{\rm FB}^{c\overline{c}} = (\ 14.7\ \pm 1.8\ \pm 0.7\ )\,\% \quad \text{at } \langle\sqrt{s}\rangle = 92.95 \text{ GeV},
\end{array}$$

and the pole asymmetries are measured to be:

$$\begin{aligned}
A_{\rm FB}^{0,\,b} &= (9.89 \pm 0.27 \pm 0.13)\,\%\,, \\
A_{\rm FB}^{0,\,c} &= (6.57 \pm 0.47 \pm 0.32)\,\%\,.
\end{aligned}$$

In all cases, the first error is statistical and the second systematic. The χ^2/dof of the fit to all OPAL asymmetry measurements to give the two pole asymmetries is 11.2/13. (There are six asymmetry measurements from the lepton tag analysis, three from the inclusive analysis, and six from the charm meson analysis, which consists of a simultaneous fit to the b and c quark asymmetries.) Taking into account statistical and systematic uncertainties, these average pole asymmetries have a +15 % correlation. Within the framework of the Standard Model, the measurements of $A_{\rm FB}^{0,\,b}$ and $A_{\rm FB}^{0,\,c}$ taken together can be interpreted as a measurement of the effective weak mixing angle for leptons of

$$\sin^2\theta_{\rm eff}^{\ell} = 0.23238 \pm 0.00052\,.$$

As can be seen from Figure 3, this result favours large values of the Higgs mass, in agreement with other measurements of heavy flavour asymmetries and in contrast to measurements of the leptonic forward-backward and left-right asymmetries [1].

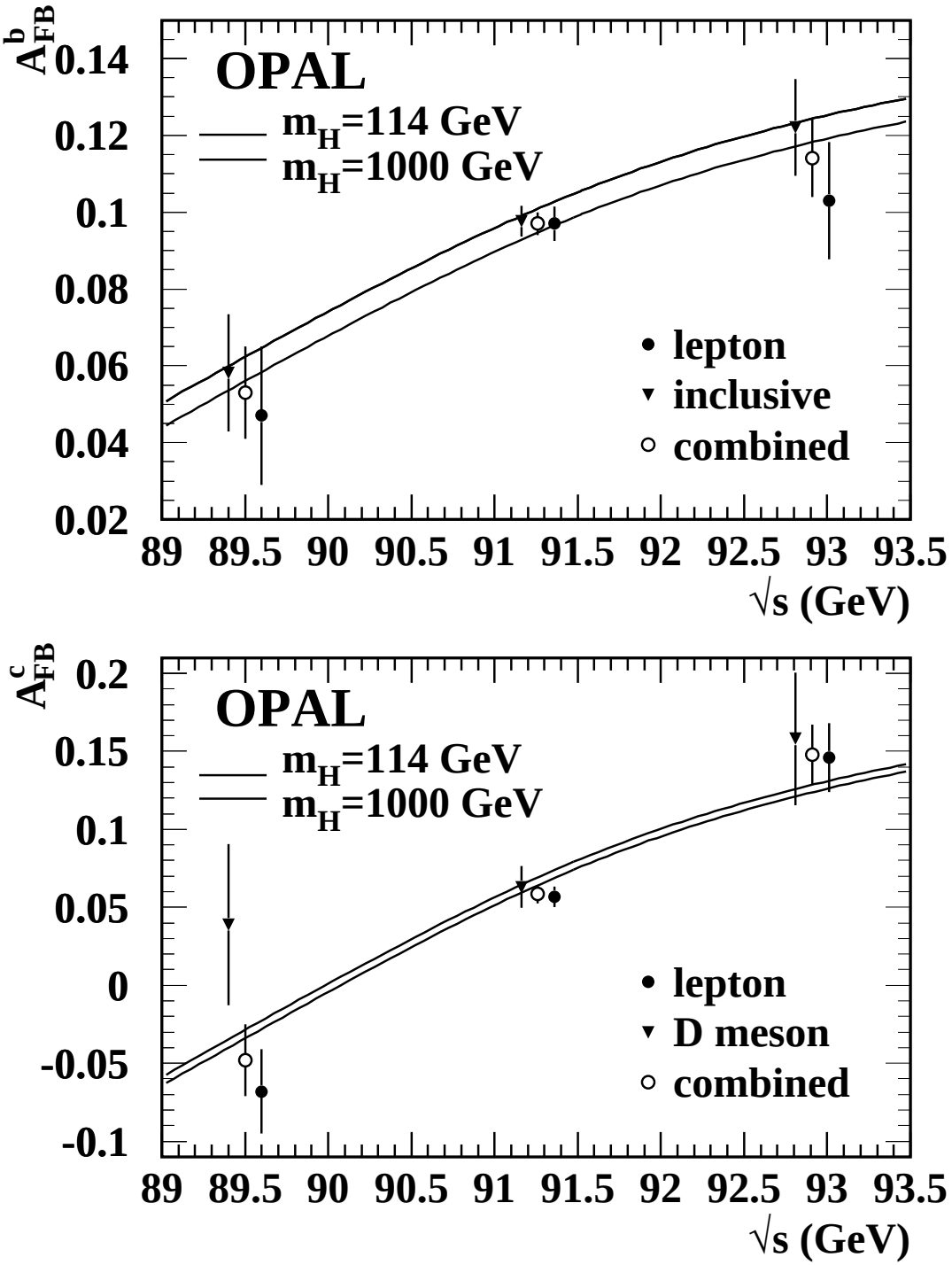

Figure 3: The measured b and c quark asymmetries as a function of centre-of-mass energy, for the lepton, inclusive (b only) [10] and D meson (c only) [13] analyses. The measurement of the b quark asymmetry from D mesons is of low precision and is not shown. The measurements from different analyses are slightly displaced on the horizontal axis for clarity. The combination of the lepton analysis and the other analyses is also shown, together with the Standard Model expectation for Higgs masses between 114 and 1000 GeV calculated using ZFITTER [28].

Acknowledgements

We particularly wish to thank the SL Division for the efficient operation of the LEP accelerator at all energies and for their close cooperation with our experimental group. In addition to the support staff at our own institutions we are pleased to acknowledge the
Department of Energy, USA,
National Science Foundation, USA,
Particle Physics and Astronomy Research Council, UK,
Natural Sciences and Engineering Research Council, Canada,
Israel Science Foundation, administered by the Israel Academy of Science and Humanities,
Benoziyo Center for High Energy Physics,
Japanese Ministry of Education, Culture, Sports, Science and Technology (MEXT) and a grant under the MEXT International Science Research Program,
Japanese Society for the Promotion of Science (JSPS),
German Israeli Bi-national Science Foundation (GIF),
Bundesministerium für Bildung und Forschung, Germany,
National Research Council of Canada,
Hungarian Foundation for Scientific Research, OTKA T-038240, and T-042864,
The NWO/NATO Fund for Scientific Research, the Netherlands.

References

[1] The LEP Collaborations, ALEPH, DELPHI, L3, OPAL, the LEP Electroweak Working Group, and the SLD Heavy Flavour Group, 'A Combination of Preliminary Electroweak Measurements and Constraints on the Standard Model', CERN-EP/2002-091, hep-ex/0212036, 17th December 2002, and references therein.

[2] Particle Data Group, K. Hagiwara *et al.*, Phys. Rev. D66 (2002) 010001.
The review includes an article by O. Schneider on $B^0\overline{B^0}$ mixing. The update using published results for the 2003 online release (`http://pdg.lbl.gov/2003/contents_listings.html`) was used here for the LEP average values of R_b and R_c.

[3] OPAL Collaboration, G. Alexander *et al.*, Z. Phys. C70 (1996) 357.

[4] ALEPH Collaboration, A. Heister *et al.*, Eur. Phys. J. C24 (2002) 177.

[5] DELPHI Collaboration, P. Abreu *et al.*, Z. Phys. C65 (1995) 569.

[6] L3 Collaboration, O. Adriani *et al.*, Phys. Lett. B292 (1992) 454;
L3 Collaboration, M. Acciarri *et al.*, Phys. Lett. B448 (1999) 152.

[7] ALEPH Collaboration, A. Heister *et al.*, Eur. Phys. J. C22 (2001) 201.

[8] DELPHI Collaboration, P. Abreu *et al.*, Eur. Phys. J. C9 (1999) 367.

[9] L3 Collaboration, M. Acciarri *et al.*, Phys. Lett. B439 (1998) 225.

[10] OPAL Collaboration, G. Abbiendi *et al.*, Phys. Lett. B546 (2002) 29.

[11] ALEPH Collaboration, R. Barate *et al.*, Phys. Lett. B434 (1998) 415.

[12] DELPHI Collaboration, P. Abreu *et al.*, Eur. Phys. J. C10 (1999) 219.

[13] OPAL Collaboration, G. Alexander *et al.*, Z. Phys. C73 (1996) 379.

[14] OPAL Collaboration, K. Ahmet *et al.*, Nucl. Instr. Meth. A305 (1991) 275;
P.P. Allport *et al.*, Nucl. Instr. Meth. A324 (1993) 34.

[15] P.P. Allport *et al.*, Nucl. Instr. Meth. A346 (1994) 476.

[16] S. Anderson *et al.*, Nucl. Instr. Meth. A403 (1998) 326.

[17] OPAL Collaboration, G. Abbiendi *et al.*, Eur. Phys. J. C8 (1999) 217.

[18] T. Sjöstrand, Comp. Phys. Comm. 82 (1994) 74.

[19] OPAL Collaboration, G. Alexander *et al.*, Z. Phys. C69 (1996) 543.

[20] C. Peterson, D. Schlatter, I. Schmitt and P.M. Zerwas, Phys. Rev. D27 (1983) 105.

[21] G. Altarelli *et al.*, Nucl. Phys. B208 (1982) 365.

[22] CLEO Collaboration, S. Henderson *et al.*, Phys. Rev. D45 (1992) 2212.

[23] DELCO Collaboration, W. Bacino *et al.*, Phys. Rev. Lett. 43 (1979) 1073.

[24] MARK III Collaboration, R.M. Baltrusaitis *et al.*, Phys. Rev. Lett. 54 (1985) 1976.

[25] J. Allison *et al.*, Nucl. Instr. Meth. A317 (1992) 47.

[26] The neural networks were trained using JETNET 3:
C. Peterson, T. Rögnvaldsson and L. Lönnblad, Comp. Phys. Comm. 81 (1994) 185.

[27] OPAL Collaboration, R. Akers *et al.*, Z. Phys. C63 (1994) 197.

[28] D. Bardin *et al.*, 'ZFITTER: An analytical program for fermion pair production in e^+e^- annihilation', CERN-TH 6443/92, hep-ph/9412201 (1992);
D. Bardin *et al.*, Comp. Phys. Comm. 133 (2001) 229;
The input parameters used were $m_Z = 91.1875\,\mathrm{GeV}$, $m_{\mathrm{top}} = 175\,\mathrm{GeV}$ and $m_{\mathrm{Higgs}} = 150\,\mathrm{GeV}$.

[29] DELPHI Collaboration, P. Abreu *et al.*, Eur. Phys. J. C14 (2000) 613.

[30] OPAL Collaboration, K. Ackerstaff *et al.*, Z. Phys. C76 (1997) 387.

[31] LEP heavy flavour working group, D. Abbaneo *et al.*, Eur. Phys. J. C4 (1998) 185.

[32] G. Altarelli and B. Lampe, Nucl. Phys. B391 (1993) 3;
V. Ravindran and W.L. van Neerven, Phys. Lett. B445 (1998) 206;
S. Catani and M.H. Seymour, JHEP 9907 (1999) 023.

[33] The LEP collaborations, ALEPH, DELPHI, L3 and OPAL, Nucl. Instr. Meth. A378 (1996) 101.
Updated averages are described in 'Final input parameters for the LEP/SLD heavy flavour analyses', LEPHF/2001-01 (see `http://www.cern.ch/LEPEWWG/heavy/`).

[34] N. Isgur, D. Scora, B. Grinstein and M. Wise, Phys. Rev. D39 (1989) 799.

[35] CLEO Collaboration, D. Bortoletto *et al.*, Phys. Rev. D45 (1992) 21.

[36] V.G. Kartvelishvili, A.K. Likhoded and V.A. Petrov, Phys. Lett. B78 (1978) 615;
B. Andersson, G. Gustafson and B. Söderberg, Z. Phys. C20 (1983) 317;
P. Collins and T. Spiller, J. Phys. G11 (1985) 1289.

[37] OPAL Collaboration, P. Acton *et al.*, Z. Phys. C58 (1993) 523.

[38] OPAL Collaboration, K. Ackerstaff *et al.*, Z. Phys. C76 (1997) 401.

[39] L. Arnaudon *et al.*, Phys. Lett. B307 (1993) 187;
R. Assmann *et al.*, Eur. Phys. J. C6 (1999) 187;
LEP energy working group, R. Assmann *et al.*, 'Evaluation of the LEP centre-of-mass energy for data taken in 2000', LEPEWG 01/01, `http://lepecal.web.cern.ch/LEPECAL/`.